INTERNATIONAL ATOMIC ENERGY AGENCY
UNITED NATIONS EDUCATIONAL, SCIENTIFIC AND CULTURAL ORGANIZATION
INTERNATIONAL CENTRE FOR THEORETICAL PHYSICS
I.C.T.P., P.O. BOX 586, 34100 TRIESTE, ITALY, CABLE CENTRATOM TRIESTE

SMR/455 - 6

EXPERIMENTAL WORKSHOP ON HIGH TEMPERATURE SUPERCONDUCTORS & RELATED MATERIALS (BASIC ACTIVITIES)

12 - 30 MARCH 1990

CERAMIC SUPERCONDUCTORS:

SINGLE-VALENT VS MIXED-VALENT OXIDES

JOHN B. GOODENOUGH

University of Texas at Austin
Center for Materials Science and Engineering
ETC 5, 160
Austin, Texas 78712
U.S.A.

(Background Material)

CERAMIC SUPERCONDUCTORS: SINGLE-VALENT VS MIXED-VALENT OXIDES

John B. Goodenough

Center for Materials Science and Engineering, ETC 5.160, University of Texas at Austin,

Austin, TX 78712-1084

The problem of electronic transport in oxides is reviewed briefly. The situation in the main-group oxides is contrasted with that in the rare-earth oxides. In $Ba_{1-x}K_xBiO_3$, for example, introduction of mixed valence allows superconductivity to compete with the charge-density wave stable in the "single-valent" stoichiometry; and in ferromagnetic EuO, oxidation leads to small-polaron conduction, but reduction gives a metal-semiconductor transition below the Curie temperature. The d-block transition-metal oxides are of intermediate character; in these oxides either localized magnetic moments or charge-density waves may compete with superconductivity. However, an abrupt transition from antiferromagnetic order to high-T_c superconductivity, such as that found in some copper oxides, is not observed in oxides where a single-band model is clearly applicable. The special features that allow for a two-band model in the high-T_c oxide superconductors are emphasized. In addition, attention is called to a thermal-expansion mismatch between A-O and B-O bonds in structures related to the ABO_3 perovskites, and the relationship of the electronic and structural features is pointed out. These special features provide the necessary framework for a strong-coupling theory of superconductivity.

INTRODUCTION

Ceramists have traditionally been more interested in refractory insulators than in metallic oxides. Consequently the report in 1986 of high-T_c superconductivity in an oxide appeared to many an especially extraordinary finding even though several oxides were already known to be superconductors.

In order to understand metallic conductivity in oxides, it is useful to consider separately three different types of atomic outer electrons: (*i*) the valence s and p electrons active in bonding, (*ii*) the rare-earth $4f^n$ manifolds that everywhere remain localized, interacting only weakly with neighboring atoms, and (*iii*) the transition-metal d electrons. The d electrons are of intermediate character: in some oxides they act like valence electrons, in others like localized electrons, and in a few they exhibit a transitional character. The latter situation occurs in the high-T_c copper-oxide superconductors; they exhibit a transition from an antiferromagnetic semiconductor in the single-valent state to superconductivity in a mixed-valent state. However, superconductivity gives way to normal metallic behavior after a relatively narrow compositional range. Any model of the superconductive properties of these copper oxides must address the question of why superconductivity occurs in only a narrow compositional range.

MAIN-GROUP OXIDES

Most main-group oxides remain refractory insulators; attempts to render them electronic conductors by chemical doping tend to be frustrated by the spontaneous incorporation of compensating native defects. The problem is well illustrated by the binary compound MgO, which has the rocksalt structure.

Construction of the electronic energies on the basis of an ionic model is illustrated in Fig. 1. The $O^{-/2-}$ redox energy for the free ion lies above the energy of vacuum E_{vac}; the formation of a free O^{2-} ion requires overcoming a negative electron affinity. The $Mg^{2+/+}$ redox energy lies below E_{vac} by the second ionization energy of magnesium. The energy E_I is the energy required to remove the remaining 3s electron from Mg^+ to an O^- ion at infinite distance to create free Mg^{2+} and

O^{2-} ions. Assembly of these ions into the rocksalt structure of MgO leads to a gain of electrostatic Madelung energy $E_M > E_I$, which stabilizes the compound. Conservation of energy lowers the $O^{-/2-}$ and raises the $Mg^{2+/+}$ redox energies by the same amount, and an $E_M > E_I$ produces a cross-over of the two energies. Introduction of covalent hybridization lowers the effective charge on the ions from their value in a point-charge model, which lowers the splitting E_M-E_I; but this lowering is compensated by the repulsion between bonding and antibonding states introduced by this hybridization. Therefore the point-charge model gives a good zero-order approximation for the binding energy of the crystal if appropriate core-core short-range repulsive energies are introduced. Finally, the translational symmetry of the crystal introduces a broadening of the energy levels into energy bands, but the bandwidths remain narrow enough to have a large energy gap E_g between a filled valence band of primarily O-2p character and an empty conduction band of primarily Mg-3s character. These bands are therefore given the formal identifications O^{2-}:$2p^6$ and Mg^{2+}:3s.

In MgO, the energy gap E_g is sufficiently large and the band edges are so positioned that the Mg^{2+}:3s conduction band is energetically inaccessible to electrons and the O^{2-}:$2p^6$ band remains inaccessible to holes. Chemical doping that would raise the Fermi energy E_F into the conduction band or would lower it into the valence band produces native defects that maintain E_F within the gap.

On the other hand, the conduction bands of heavy Group B metals in higher valence states are energetically accessible. Although the Sn^{4+}:5s conduction band of SnO_2 lies 3eV above the O^{2-}:$2p^6$ valence band, nevertheless it can be doped to give a metal that is transparent, and the PbO_2 cathode of a lead-acid battery is metallic even without the injection of hydrogen on discharge.

The situation is illustrated in Fig. 2 for three cubic perovskites: $BaSnO_3$, $BaPbO_3$, and the hypothetical $BaBiO_3$. Stoichiometric $BaSnO_3$ is a semiconductor because the Sn^{4+}:5s conduction band lies discretely above the O^{2-}:$2p^6$ valence band, as in SnO_2; $BaPbO_3$ is a semimetal because the Pb^{4+}:6s and O^{2-}:$2p^6$ bands overlap, as in PbO_2. Cubic $BaBiO_3$ would have a greater overlap of the "Bi^{4+}:6s" and O^{2-}:$2p^6$ bands, but the conduction band would be half filled, thereby raising E_F above the top of the valence band. Clearly an ionic model becomes less appropriate for these

heavy B metal oxides where a small E_M-E_I implies strong covalent mixing between the metal 6s and oxygen-2p orbitals and the bandwidths cause E_g to disappear.

The situation in the hypothetical cubic $BaBiO_3$ must be distinguished from the other two cases because the Bi:6s conduction band is half filled. The electronic energies of a partially filled band can be stabilized by a change in the translational symmetry that lowers the energies of occupied states at the expense of unoccupied states by opening up an energy gap at the Fermi surface. Where this energy gain exceeds the elastic restoring energy that favors higher symmetry, a semiconductor-metal transition can be expected below some critical temperature T_t (1). Alternatively, the electron-phonon interactions can stabilize the condensation of Cooper pairs below a superconductive critical temperatuare T_c. Thus the lattice instabilities responsible for semiconductor-metal transitions below T_t are competitive with the stabilization of superconductivity.

It is well known to chemists that Bi^{4+} is not a stable valence state; it is unstable against the disproportionation reaction

$$2Bi^{4+} \rightarrow Bi^{3+} + Bi^{5+} \qquad (1)$$

Thus it comes as no surprise that cubic $BaBiO_3$ does not exist at room temperature. As illustrated in Fig. 3, the oxygen atoms are cooperatively displaced so as to create two distinguishable Bi atoms, a Bi_I with larger Bi-O distances and a Bi_{II} with shorter Bi-O distances. There is also a cooperative tilting of the octahedra relative to a [100] axis that lowers the symmetry from cubic to monoclinic. These displacements clearly signal a disproportionation reaction that may be described as

$$2Bi^{4+} \rightarrow Bi_I^{(4-\delta)+} + Bi_{II}^{(4+\delta)+} \qquad (2)$$

where $\delta = 1$ would correspond to a classic disproportionation into Bi^{3+} and Bi^{5+}. In fact, a $\delta = 0.5$ is found (2); a $\delta < 1$ represents a charge-density wave (CDW). No matter what the value of δ, the creation of two distinguishable Bi sites by the freezing out of a vibrational breathing mode changes the translational symmetry of the crystal so as to split the conduction band in two, leaving the Fermi energy E_F in an energy gap. $BaBiO_3$ is thereby rendered a semiconductor.

Stabilization of a polar state on the Bi-atom array is only possible because the electrostatic correlation energy U between Bi-6s electrons, which is the energy cost to create a non-uniform distribution of charge, is smaller than the gain Δ in covalent-hybridization energy associated with the motion of the oxygen atoms towards one Bi atom and away from the other (1). In the physics literature, a $\Delta > U$ is referred to as a "negative U," i.e. a $U_{eff} = U - \Delta < 0$. This condition can be stable only where the free-atom U is relatively small, as for the Bi-6s electrons, and even there only for a range of bandwidths as is illustrated schematically in Fig. 4.

If K is substituted for Ba in $Ba_{1-x}K_xBiO_3$, the BiO_3 framework becomes oxidized. As the Bi-6s conduction band becomes less than half-filled, the wavelength **q** of the CDW that opens up a gap at E_F increases and the stabilization energy of the CDW decreases, lowering the semiconductor-metal transition temperatuare T_t (). In fact, **q** need not remain commensurate with the periodicity of the crystal structure, and the $Ba_{1-x}K_xBiO_3$ system exhibits a monoclinic-tetragonal transition with increasing x that probably represents a transition from a commensurate to an incommensurate CDW (). As the K-substituted phases are difficult to synthesize, the phase diagram of Fig. 5 must be considered tentative. A single crystal with $x = 0.13$ was found to be cubic at room temperatuare and to exhibit no magnetic anomaly characteristic of superconductivity down to lowest temperatuare (), but it was inadvertently destroyed before a T_t could be measured in the sample. However, near $x = 0.25$ there is an abrupt onset of superconductivity with a T_c that decreases monotonically with increasing x over the narrow compositional interval $0.25 < x < 0.5$. A two-phase region probably separates the CDW and superconductor compositions, but this feature has not yet been established.

Although the $Ba_{1-x}K_xBiO_3$ superconductors appear to be described by the Bardeen-Cooper Schrieffer (BCS) weak-coupling theory (), they exhibit a T_c that is higher than expected from that theory for the measured density $N(E_F)$ of one-electron states at the Fermi energy. Therefore this system is classified with the high-T_c copper-oxides as representative of anomalous superconductivity. In this respect it differs from the other known oxide superconductors such as

TiO and $Li[Ti_2]O_4$. Moreover, confinement of superconductivity to a narrow compositional range, i.e. a narrow electron-atom ratio, is a striking feature that has not yet been addressed theoretically.

Examination of Fig. 2(c) is instructive. Oxidation of the BiO_3 array lowers E_F toward the top of the O-$2p_\pi$ band; experimental evidence that E_F lies within the O-$2p_\pi$ band in the superconductor composition $x = 0.4$ is now available (8). We will see that a distinguishing feature of a high-T_c oxide superconductor is an E_F that cuts two bands, a π or π^* band of primarily O-$2p_\pi$ character and a σ^* band of primarily cationic (Bi-6s or Cu-3d) character. In the other oxide superconductors such as TiO or $Li[Ti_2]O_4$, E_F cuts a single cationic d band. The possible significance of this distinguishing feature is discussed in a final speculative comment.

RARE-EARTH OXIDES

The 4f electrons of the rare-earth ions are tightly bound to their atomic nucleus and are screened from interactions with neighboring atoms by the $5s^25p^6$ closed-shell core electrons. As a result, the intraatomic interactions among the 4f electrons of the $4f^n$ configuration are much smaller than the interatomic 4f-4f interactions. Consequently the Hamiltonian describing a $4f^n$ configuration has the form

$$H = H_o + V_{el} + \Delta_{LS} + \Delta_{cf} + H_z \qquad (3)$$

where H_o is the spherical approximation and the successive terms represent successive perturbation corrections to this approximation. The first three terms, which include the electrostatic covalent interactions between the 4f electrons (V_{el}) and the spin-orbit coupling ($\Delta_{LS} = \lambda \underset{\sim}{L} \cdot \underset{\sim}{S}$) responsible for multiplet splittings, are present in the free atom and give rise to an atomic magnetic moment

$$\mu_J = gJ\mu_B \qquad (4)$$

where g is the Landé spectroscopic splitting factor. The energy V_{el} gives rise to the splittings U_n between successive $4f^n$ configurations, i.e. $4f^n$ and $4f^{n+1}$. Because the radial extension of the 4f electrons is relatively small, the energies U_n are large, $U_n > E_g$ where E_g is the energy gap between the top of the O-2p valence band and the bottom of the Ln-5d conduction band.

(Stronger covalent mixing of the O-2p orbitals with Ln-6s vs Ln-5d orbitals raises the bottom of the Ln-6s band above the bottom of the Ln-5d band).' A $U_n > E_g$ restricts the number of energetically available $4f^n$ configurations to one or, at most, two; two are accessible only if a $4f^n$ configuration has its energy falling within E_g.

The last two terms in Equation (3) are the crystal-field splitting Δ_{cf}, which is primarily due to Ln-4f interactions with the nearest-neighbor oxide ions, and the Zeeman splitting H_z due to the internal magnetic fields produced by interatomic magnetic-exchange interactions with nearest-neighbor magnetic atoms. Because Δ_{cf} and H_z are both weaker than Δ_{LS}, the effective atomic magnetic moment μ_{eff} obtained from magnetic-susceptibility measurements provides an excellent measure of the $4f^n$ configuration at a rare-earth ion. Since any 5d electrons present act like valence electrons, the "valence" of a rare-earth ion is generally defined as the total number of outer electrons on the atom minus the number n of the ground-state $4f^n$ configuration.

Some consequences of these considerations are illustrated in Fig. 6 for GdO and EuO, each with the same rocksalt structure as MgO. The valence $O^{2-}:2p^6$ and conduction Ln:5d bands are constructed in a manner analogous to the construction of the valence and conduction bands of MgO, but with differential covalent mixing of O-2p with Ln-6s and 5d orbitals rendering the bottom of the conduction band Ln:5d in character. The splitting U between $4f^8$ and $4f^7$ energy levels is particularly large because the $4f^7$ configuration just completes the half-shell. The $4f^7$ level for Gd falls well below the top of the valence band, and the $4f^8$ energy lies well above the bottom of the conduction band. Therefore only the $4f^7$ level can be occupied, and the Gd has the formal valence Gd^{3+} according to the magnetic criterion. However, each Gd can transfer at most two electrons to the oxygen, so the third valence electron occupies the Gd-5d conduction band, and GdO is a metallic antiferromagnet, the interatomic antiferromagnetic exchange being indirect through the intinerant 5d electrons. In EuO, on the other hand, the $Eu^{2+}:4f^7$ configuration lies in an energy gap about 1.1 eV below the bottom of the Eu 5d conduction band. Therefore EuO is a semiconductor that can be doped both n-type and p-type since both the Eu 5d and Eu-$4f^7$ energies are accessible (9). Moreover, the dominant interatomic magnetic exchange is ferromagnetic via a $Eu:4f^7 - Eu:5d$ superexchange interaction, and EuO is a ferromagnet at low temperature.

Oxidation of EuO to $Eu_{1-\delta}O$ introduces cation vacancies and lowers E_F into the narrow $Eu^{2+}:4f^7$ level, which represents the $Eu^{3+/2+}$ redox energy. Because the 4f electrons are localized, the electron transfer reaction

$$Eu^{3+} + Eu^{2+} \rightleftharpoons Eu^{2+} + Eu^{3+} \qquad (5)$$

is low relative to the period of an optical-mode vibration ($\tau_h > \omega_R^{-1}$), which means that the empty $4f^7$ energy at a Eu^{3+} ion is raised above the occupied $4f^7$ energy at a Eu^{2+} ion by a local reorganization energy. The situation is completely analogous to the redox energies of an ion in solution except that the periodicity of the crystal structure requires a configuration mobility that averages the electron occupancy at a given Eu atom over time. The mobile electron (or hole in this case) and its local deformation is called a "small polaron." Since it has a diffusive motion, its drift mobility is given by the Einstein relation

$$\mu = e_o D/kT = (e_o D_o/kT)\exp(-\Delta G_m/kT) \qquad (6)$$

where e_o is the magnitude of the electronic charge and $\Delta G_m = \Delta H_m - T\Delta S_m$ is the motional free energy. The motional enthalpy ΔH_m is a measure of the magnitude of the local reorganization energy. Since the electronic conductivity is related to the electron mobility via the relation

$$\sigma = pe_o\mu \qquad (7)$$

where p is the concentration of mobile holes, it follows that the conductivity of $Eu_{1-\delta}O$ retains an activation energy through μ even where p is independent of temperature, so the mixed-valent system also exhibits semiconductor behavior.

Reduction of EuO to $EuO_{1-\delta}$ produces oxygen vacancies V_O that stabilize a two-electron trap state from out of the conduction band (10). This situation differs from phosphor-doped silicon, where the donor state is a single-electron trap. Because the trap states are condensed out of the conduction band, their energies ride with the bottom of the conduction band. On cooling through the ferromagnetic Curie temperature T_c, states with spins parallel to the spin of the $4f^7$ configuration (α spin direction) have their energies shifted relative to the states of opposite spin (β

spin direction) by $2\mu_B H_i$, where H_i is the internal molecular field due to the interatomic magnetic-exchange interactions. The two electrons trapped at an oxygen vacancy have opposite spins, so one rides with the bottom of the α spin band and the other with the bottom of the β spin band. The energy of the α-spin donor state is lowered by U_t in a single-electron trap. As the spontaneous magnetization M_s increases below T_c, H_i increases; at a critical value of M_s the β-spin donor energy crosses the bottom of the α-spin conduction band. As the temperature continues to decrease, the β-spin donor electrons are emptied into the α-spin conduction band; these conduction electrons increase T_c, thereby increasing M_s, which produces a positive feedback that results in a sharp semiconductor to metal transition with decreasing temperature. The electrons in the conduction band are itinerant ($\hbar/\tau_s < \omega_R$), so there is no local reorganization to trap them; therefore, their mobility is given by the expression

$$\mu = e_0\tau_s/m^* \tag{8}$$

where m^* is the electron effective mass and τ_s is the mean-free time between scattering events. With a fixed mobile-electron concentration and a mobility that decreases with increasing temperature because scattering from phonons increases in probability with temperature, the electronic conductivity has a metallic character.

TRANSITION-METAL (d-BLOCK) OXIDES

A description of the outer d electrons at transition-metal cations in an oxide begins with the recognition that the d orbitals interact much more strongly with neighboring atoms than the 4f orbitals, but not as strongly as the outer s and p orbitals. Whereas the interatomic interactions give a bandwidth $W > U$ for the s and p electrons, but a $(\Delta_{cf} + H_{so}) < \Delta_{LS}$ for the 4f electrons, the d electrons are of intermediate character; they have a cubic component Δ_c of the crystalline field splitting Δ_{cf} and a bandwidth W due to interactions with other transition-metal atoms that may be comparable to or even greater than the V_{el} term responsible for the interatomic correlation splitting U between d^n and d^{n+1} manifolds. It is therefore generally useful to begin with the influence of

the cubic component of the crystalline field Δ_c due to interactions with the nearest neighbor oxide ions as expressed by the Hamiltonian

$$H = H_o + (V_{el} + \Delta_c) \tag{9}$$

By symmetry, the cubic component of the crystalline field splits the fivefold degeneracy of the d orbitals into two accidentally degenerate groups, the twofold-degenerate e orbitals having the angular dependences

$$f_e \sim \frac{1}{\sqrt{2}}[(z^2-x^2) + (z^2-y^2)]/r^2 \text{ and } (x^2-y^2)/r^2 \tag{10}$$

and the threefold-degenerate t_2 orbitals having the angular dependences

$$f_t \sim (yz \pm izx)/r^2 \text{ and } xy/r^2 \tag{11}$$

This splitting quenches the azimuthal orbital angular momentum $L_z = -i\hbar\,\partial/\partial\phi$ associated with the atomic d orbitals $[(x^2-y^2) \pm ixy]/r^2$. Covalent hybridization is introduced by allowing a virtual electron transfer from an O^{2-} ion to an empty d orbital; from second-order perturbation theory, the covalent-mixing parameter λ is given by

$$\lambda = b^{ca}/\Delta E \tag{12}$$

where b^{ca} is the cation-anion resonance integral (electron-transfer-energy matrix element) and ΔE is the energy separation of the acceptor and donor orbitals of the charge transfer. The result of this covalent hybridization for octahedral-site coordination is (3)

$$\Delta\epsilon = \Delta_M + \frac{1}{2}(\lambda_\sigma^2 - \lambda_\pi^2)\,\Delta E_1 + \frac{1}{2}\lambda_S^2\,\Delta E_2 \tag{13}$$

where Δ_M is a relatively small electrostatic component, ΔE_1 and ΔE_2 are the energy separation of the empty cation-d^{n+1} configuration and the O-2p donor and the O-2s donor orbitals, and the subscripts σ, π, s refer to mixing with O-$2p_\sigma$, O-$2p_\pi$, and O-2s orbitals, respectively. The crystal-field wave functions having e-orbital and t_2-orbital symmetry in octahedral-site coordination are

$$\psi_e = N_\sigma(f_e - \lambda_\sigma\phi_\sigma - \lambda_{-\sigma}\phi_{-\sigma}) \tag{14}$$

$$\psi_t = N_\pi(f_t - \lambda_\pi\phi_\pi)$$

where the ψ_i are the appropriately symmetrized O-2s, O-$2p_\sigma$, and O-$2p_\pi$ orbitals. Extension of the d wave functions out over the anions via the covalent mixing accomplishes two important things:

(*i*) it reduces the parameter U from its value for the free ion to that more nearly given by successive redox potentials for the hydrated cation in aqueous solutions, and (*ii*) it allows important interatomic cation-anion-cation interactions to occur.

The next step in the problem is to consider the relative magnitudes of Δ_c and the difference Δ_{ex} in V_{el} for high-spin vs low-spin configurations. A high-spin configuration ($\Delta_c < \Delta_{ex}$) is only found where the d orbitals are sufficiently localized to impart a localized magnetic moment to the transition-metal cation.

Once these intraatomic energy considerations have been obtained, it is then necessary to consider the interatomic interactions between like atoms, which introduce a bandwidth W to the configuration d^n. If the condition W < U holds, then the d^n configuration is localized and imparts a localized magnetic moment to the transition-metal atoms. In the limit $W < \Delta_{LS} < U$, the interatomic exchange interactions in a single-valent compound are treated by second-order perturbation theory; this treatment gives rise to the superexchange spin-spin interaction. For half-filled orbitals, this latter interaction is antiferromagnetic, the corresponding magnetic-ordering (Néel) temperature is

$$T_N \sim b^2/U_{eff} \tag{15}$$

where $b \approx \varepsilon\lambda^2$ for cation-anion-cation interactions and $b = \varepsilon \exp(-R/\rho)$ for cation-cation interactions. In these expressions, ε is a one-electron energy, R is the interatomic separation, and ρ is a parameter in units of R. The energy

$$U_{eff} = U' + \begin{cases} 0 \\ \Delta_{ex} \\ \Delta_c \end{cases} \tag{16}$$

includes any contribution from Δ_c or Δ_{ex} that must be added for a particular value of n in the d^n configuration (11).

This localized-electron picture applies to the $3d^5$ configuration of a Mn^{2+} ion in the antiferromagnetic insulator MnO, and construction of an energy diagram proceeds as outlined in Fig. 7. In this case, the Madelung stabilization raises the Mn^{2+}:d^5 configuration as well as the

Mn^{2+}:4s energies above the top of the O^{2-}:$2p^6$ band. The energy separation U of the $3d^6$ and $3d^5$ configuration is large because $U_{eff} = U' + \Delta_{ex}$ applies on adding an electron to a set of half-filled orbitals as is found in the high-spin $d^5 = t_2^3e^2$ configuration. On the other hand, the energy separation between the $3d^5$ and $3d^4$ configurations is only $U_{eff} = U'$, which is relatively small for the crystal-field ψ_e orbitals. Thus both the $Mn^{3+/2+}$ and $Mn^{4+/3+}$ redox energies lie above the top of the O^{2-}:$2p^6$ valence band, so the three valence states Mn^{2+}, Mn^{3+}, and Mn^{4+} are chemically accessible in oxides (see also Fig. 8). However, a $U_{eff} = U' + \Delta_c$ lowers the $3d^3$ configuration below the top of the O^{2-}:$2p^6$ band, so it is not possible to oxidize manganese beyond Mn^{4+} in an octahedral interstice of an oxide. Note that the relatively small U' separating the $3d^4$ and $3d^5$ configurations makes it possible for a "negative-U" disproportionation to occur:

$$2Mn^{3+} \rightarrow Mn^{2+} + Mn^{4+} \tag{17}$$

However, in practice this reaction is only found at the surface of a manganese oxide, e.g. in strong acidic media it allows $Li[Mn_2]O_4$ to be transformed to λ - MnO_2 (12).

The superconductor TiO corresponds to a single-valent compound having W > U', where $U_{eff} = U'$ for a $3d^2$ configuration in an octahedral interstice. For a W > U', the 3d electrons are itinerant, and tight-binding band theory must be applied to the electrons in the crystal-field ψ_t orbitals. The resulting density-of-states curve N(E) for TiO (we neglect the spontaneous introduction of atomic vacancies in the structure) is compared to that of MnO in Fig. 8. By contrast, VO contains a half-filled set of t_2 orbitals (V^{2+}:$t_2^3e^0$), so $U_{eff} = U' + \Delta_c$ is larger. Nevertheless the bandwidths of the $V^{3+/2+}$ and $V^{4+/3+}$ redox energies overlap ($W \geq U$), so the compound is semi-metallic. Nevertheless there is a deep minimum in the N(E) vs E curve. In this case, the correlation splitting U is large enough to introduce an important enhancement of the Pauli paramagnetic susceptibility, but the compound remains metallic with no vanadium magnetic moments, and hence no antiferromagnetic order, at low temperatures.

For a half-filled band, these considerations lead to the phase diagram of Fig. 9, which shows a transition from an antiferromagnetic semiconductor for $b < b_c$, i.e. W < U, where there are localized magnetic moments on the cations, to a Pauli-paramagnetic metal for $b > b_c$, i.e. W >

U, where the existence of a Fermi surface at E_F allows for a transition to superconductivity below a T_c given by the weak-coupling BCS theory. It is immediately apparent from this figure that, with a single-band model, the presence of spontaneous magnetic moments associated with a correlation splitting U > W is incompatible with superconductivity.

Again we must ask what happens when the system is changed form a single-valent to a mixed-valent configuration. Oxidation, for example, would lower E_F into the lower of the correlation-split bands and reduction would raise it into the upper of the correlation-split bands. In this case it is necessary to distinguish whether the partially filled band, according to the Heisenberg Uncertainty principle, gives rise to an electron-hopping time between neighboring atoms

$$\tau_h = \hbar/\tfrac{1}{2}W \qquad (18)$$

that is long or short compared to the period ω_R^{-1} of the optical-mode vibration that would trap it -- by a small-polaron reorganization energy -- in a local deformation. As illustrated in Fig. 10, the mixed-valent spinel $Li[Mn_2]O_4$ contains small polarons and retains localized magnetic moments on the Mn atoms whereas isostructural $Li[Ti_2]O_4$ is metallic and a superconductor. Also shown are the N(E) vs E curves for A_xMO_3 bronzes (M = Mo or W) that are metallic superconductors as a result of strong M-O-M interactions; in $Li[Ti_2]O_4$ the strong interatomic interactions are Ti-Ti interactions across shared octahedral-site edges.

Of course CDW transitions can occur in transition-metal oxides with W > U. This situation is richly illustrated in the chemistry of the molybdenum oxides (13). But my purpose now is to turn to the high-T_c copper-oxide superconductors.

HIGH-T_c COPPER OXIDES

All the high-T_c copper-oxide superconductors have a common structural feature: they contain intergrowths of copper oxide layers and other oxides. The simplest of these structures is the tetragonal phase of Fig. 11(a), which is the room-temperature structure of $La_{1.85}Sr_{0.15}CuO_4$ having a $T_c \approx 40K$. Between room temperature and T_c, the structure undergoes a displacive

transition to orthorhombic symmetry in which the tetragonal (c/a > 1) CuO_6 octahedra rotate cooperatively as indicated in Fig. 11(b) (14,15). This simplest of the cuprate superconductor systems will serve to illustrate the essential features I wish to consider.

The phase diagram for the system $La_{2-x}Sr_xCuO_4$ is shown in Fig. 12 for $0 \le x \le 0.4$; to retain a full oxygen content with ~~x > 0.15~~, it is necessary to prepare the samples under high oxygen pressure (*ca* 3kbar) (16-18). Five features should be noted: (*i*) La_2CuO_4 itself is orthorhombic at room temperature and an antiferromagnetic semiconductor. (*ii*) In the compositional range $0 < x < 0.08$, the antiferromagnetic-ordering temperatuare T_N decreases sharply with increasing x, disappearing at a semiconductor-metal boundary -- probably a narrow two-phase region. (*iii*) Superconductivity is confined to a narrow compositional range $0.1 \le x \lesssim 0.3$ within which the system becomes orthorhombic below a $T_t > T_c$. (*iv*) Dynamic, short-range antiferromagnetic fluctuations have been observed (19) in the superconductor compositions, the coherence length decreasing with increasing x and the spin fluctuations exhibiting no change as the temperature was reduced through T_c. (*v*) The normal-metal state changes from p-type to n-type on doping beyond the superconductive compositional range.

In Fig. 13(a) is shown a schematic representation of the one-electron density of states N(E) vs energy E as calculated from band theory for La_2CuO_4 (20-22). However, La_2CuO_4 is antiferromagnetic with a copper magnetic moment $\mu_{Cu} = 0.5\ \mu_B$ (23,24). Consequently it is necessary to amend the diagram by the introduction of a correlation splitting of the σ^* band as shown in Fig. 13(b). From the tetragonal (c/a > 1) symmetry of the CuO_6 octahedra, the top of the σ^* band has $3d_{x^2-y^2}$ parentage (z-axis parallel to c-axis), but with strong covalent hybridization with the O-$2p_x$ and O-$2p_y$ σ-bonding orbitals in the CuO_2 planes. The observation of a copper magnetic moment shows that the empty σ^* band states are primarily Cu-3d in character, which means an $E_M > E_I$ applies for the σ-bonding orbitals, where the energies E_M and E_I have the same meaning as in Fig. 1, but with the second electron removed from copper originating from the Cu-$3d_{x^2-y^2}$ orbital. However, with a

$$U_{eff} = U' + \Delta_t > W_\sigma$$

where A_1 is the tetragonal component of A_{1g}, it is necessary to inquire whether an $E_M > E_I$ can still apply on deeper oxidation of the system.

It is now established from spectroscopic evidence that, in all the p-type copper oxide superconductors, oxidation creates mobile holes in π^* - band states that are primarily O-$2p_\pi$ in character, the particular $2p_\pi$ orbitals being the p_x and p_y π-bonding orbitals of the oxygen atoms in the CuO_2 planes (25,26). How this can be so is illustrated schematically in Fig. 13(c). This peculiar situation arises because of the cross-over from $E_M > E_I$ for Cu^{2+} to $E_M < E_I$ for Cu^{3+}. The correlation splitting of the σ^* band ensures that, on oxidation, E_F drops into the π^* band rather than into the lower σ^* band. Moreover, the observation of short-range spin fluctuations on the copper in the superconductive phase shows the persistence of this correlation splitting to higher values of x in $La_{2-x}Sr_xCuO_4$. Preliminary XPS data (23) show that for $x > 0.3$, where the system remains tetragonal and a normal metal to lowest temperatures, E_F moves out of the π^* band into only the σ^* band as the correlation splitting becomes $U < W_\sigma$, where Fig. 13(a) applies. Without the correlation splitting, the holes should be stabilized in the σ^* -band states as these are the most strongly antibonding. The $\sigma^*_{x^2-y^2}$ band is less than half-filled, so the charge carriers are n-type.

Thus we can conclude that a common feature of the electronic structure of the high-T_c $Ba_{1-x}K_xBiO_3$ and $La_{2-x}Sr_xCuO_4$ (and other copper-oxide systems as well) is a Fermi energy that intersects two bands, a σ^* band of primarily cationic character (Bi-6s or Cu-3d) and a π or π^* band of primarily O-$2p_\pi$ character. The mobile holes in the π^* bands are responsible for the superconductivity in the copper oxides (27); they make possible an abrupt transition from an antiferromagnetic semiconductor to a superconductor with increasing oxidation, and from a superconductor to a normal metal where the mobile holes are transferred to the σ^* band.

In this connection, attention should be drawn to the evidence for a sharp transition in the Cu-O bond length on going from the antiferromagnetic state to the superconductive state (28,29). In the case of the superconductor phase $La_2CuO_{4.05}$ -- prepared at 800°C under 23 kbar pressure in a double cell consisting of CrO_3 on one side of a $Zr_{1-x}Ca_xO_{2-x}$ separator and the sample on the other--heating in air yields a first-order phase change to antiferromagnetic La_2CuO_4 with loss of

oxygen (28). The excess oxygen is incorporated as O^{2-} ions in the tetrahedral sites of the double La_2O layers of Fig. 11(a) (30,31) where it oxidizes the CuO_2 layers (25). The change in lattice parameters on traversing the transition is shown in Fig. 14. Note the increase in the a-axis on passing from the superconductor to the antiferromagnetic semiconductor. The increase in Cu-O distance is even more marked as the tilting of the CuO_6 octahedra is greater in the antiferromagnetic phase. The shorter Cu-O distance is reflected in a stronger Cu-O-Cu interaction, which moves the system to the right from a $b_\sigma < b_g$ in the energy-band diagram Fig. 9 for the half-filled $\sigma^*_{x^2-y^2}$ band; in fact, it appears to move b_σ to a $b_\sigma \geq b_g$. Such a change would not normally introduce superconductivity; any band exhibiting short-range antiferromagnetic correlations would have a deep minimum in the N(E) vs E curve, which would suppress T_c according to conventional BCS theory. ~~Suppression of the copper magnetic moment μ_{Cu} is a necessary, but not a sufficient condition for high-T_c superconductivity.~~

The discussion thus far has concentrated on the electronic properties that may be peculiar to the high-T_c copper oxides. We have found evidence for an important increase in the strength of the Cu-O-Cu interactions in the CuO_2 sheets, and hence for a suppression of the copper magnetic moment, on passing from an antiferromagnetic phase to a superconductor phase on oxidation from $(CuO_2)^{2-}$. Where the Cu-O-Cu bond angles are bent from 180°, the mobile holes responsible for the high-T_c superconductivity occupy π^* -band states of primarily O-$2p_\pi$ character; where the bond angles are 180°, the holes occupy σ^* -band states and the p-type oxides exhibit normal metallic behavior to lowest temperatures. In copper oxides with the $YBa_2Cu_3O_{6+x}$ structure, the CuO_2-Y-CuO_2 layers containing double CuO_2 sheets retain bond angles that are bent from 180° at all oxidation states, and T_c is found to increase with the concentration of mobile holes ~~in the π^* bands~~ (32). We have also argued that where the Fermi energy cuts both a π^* and a σ^* band, there the orbital hybridizations that optimize Cu-O bonding and bond angles can readily adjust themselves -- via electron-lattice coupling -- into bond changes associated with lattice vibrations. We have referred to these hybridization fluctuations as "polarization fluctuations" (33). On the

other hand, such a model infers a strong coupling of the superconductive Cooper pairs via a strong electron lattice interaction yet to be identified.

STRUCTURAL CONSIDERATIONS

To address the remaining questions, it is necessary to return to structural considerations.

The high-T_c oxide superconductors all have structures related to that of perovskite, $CaTiO_3$. The ideal ABO_3 cubic perovskite contains a simple-cubic BO_3 framework of corner-shared octahedra with the A cation at the center of the unit-cell cube. A variety of displacive transitions to lower symmetry are known (34); $CaTiO_3$, for example, is orthorhombic at room temperature as a result of a cooperative buckling of the TiO_3 framework that optimizes the Ca-O bonding.

The perovskite structure is remarkable in two fundamental respects: (*i*) It may sustain large concentrations of vacancies on any of the three atomic arrays; many of the high-T_c copper-oxide phases not discussed contain ordered oxygen vacancies, for example. (*ii*) On traversing a [001] axis, BO_2 planes alternate with rocksalt-type AO planes; this structural feature requires a matching of bond lengths that, once met, allows ready stabilization of intergrowth structures. The La_2CuO_4 structure is the simplest example of such an intergrowth structure.

The criterion for bondlength matching has been traditionally expressed by the Goldschmidt tolerance factor

$$t = (r_A + r_O)/\sqrt{2}(r_B + r_O)$$

where r_A, r_B and r_O are the respective ionic radii. A $t = 1$ corresponds to a perfect epitaxial match for intergrowth of (AO) rocksalt layers with BO_2 planes. However, it must be stressed that the thermal expansions of the softer A-O bonds are greater than those of the B-O bonds, so the factor t decreases with decreasing temperature. The existence of a $t = 1$ at the firing temperature in a high-temperature synthesis may allow the structure to form, but at lower temperatures the B-O bonds are subjected to a compressive stress and the A-O bonds to a tensile stress. This bond mismatch can be relieved by a displasive transition such as the octahedral site buckling found in $CaTiO_3$.

In La_2CuO_4, the distortion from tetragonal to orthorhombic symmetry represents an improvement of the bondlength matching; the La-O bondlengths are decreased and the Cu-O bondlengths are increased by the tilting of the CuO_6 octahedra. If the smaller Nd^{3+} ion is substituted for La^{3+}, the bondlength mismatch is accommodated by a removal of the c-axis oxygen to the plane of tetrahedral sites of Nd^{3+} ions, thus creating a fluorite-type intergrowth layer. In this structure, Fig. 15, the Cu-O-Cu bond angle is 180°, and the oxide does not become a superconductor if these CuO_2 layers are oxidized (35). However,it does become a superconductor if these layers are reduced (36-39).

What is remarkable is that all of the p-type superconductors (those that become superconductors on oxidation) have Cu-O-Cu bond angles < 180°. Moreover, the disappearance of superconductivity with increasing x in the system $La_{2-x}Sr_xCuO_4$ is associated with the disappearance of the orthorhombic distortion at a $T_t > T_c$. Even the superconductor $La_2CuO_{4.05}$, which is nearly tetragonal at room temperature, becomes orthorhombic at a $T_t > T_c$.

In addition to this structural correlation, the copper-oxide superconductors are characterized by a small coherence length ($\xi \sim 10$ Å) and a weak isotope effect, which are characteristic of the strong-coupling limit where it should be possible to think about the coupling of Cooper pairs in potential wells created by real-space lattice deformations. The structural correlations appear to provide a clue as to what those real-space lattice deformations may be.

Consider first a p-type orthorhombic $La_{1.85}Sr_{0.15}CuO_4$. The orthorhombic distortion is created to relieve the compressive stress on the Cu-O bondlength. In this situation, Sr^{2+} substitution for a smaller La^{3+} ion relieves this stress -- and hence reduces the magnitude of the orthorhombic distortion -- both by increasing the mean A-O bondlength and by introducing holes -- O-$2p_\pi$ holes -- into the Cu-O bonds. In this environment, a hole in the antibonding π^* bands of O-$p_{x,y}$ and Cu-$d_{x^2-y^2}$ parentage would shorten the Cu-O bondlength in the basal plane and thus would tend to increase the Cu-O-Cu bond angle toward 180°; therefore, a cooperative change in the bond angle within a restricted area of a CuO_2 sheet would tend to localize the hole to that area of the sheet. The extended hole and associated lattice deformation would represent a "large

polaron" because the hole would be trapped in a region including multiple Cu and O centers. The mobility of a large polaron is not activated, it moves with a momentum vector **k** that remains a good quantum number. Collision with a second large polaron of momentum -**k** and opposite spin creates a reinforced potential well in which the hole pair becomes trapped as a "large bipolaron." In an external electric field, the potential well with its two trapped holes moves, in the superconducting state, with a drift velocity without scattering by the phonons of the crystal. What makes strong the coupling between the paired holes is an enhancement of the electron-lattice coupling (*i*) by the internal stresses built into the system due to a bondlength mismatch and (*ii*) by the relief of this stress with a bending of the Cu-O-Cu bond and easy bond rehybridization. Only if the Cu-O-Cu angle is bent from 180° can the structure respond strongly to the stress relief associated with π^* -band holes.

In Nd_2CuO_4, the 180° Cu-O-Cu bonds tend to be stretched, so there can be no potential well associated with a hole. Lengthening of the Cu-O-Cu bondlength reduces the Cu-O-Cu interactions, which keeps a $b_\sigma < b_g$ and hence a copper magnetic moment. However, introduction of electrons into the upper σ^* band relieves any tensile stress in the Cu-O-Cu bonds and creates a mixed valence on the copper that lowers the critical bandwidth for a spontaneous copper magnetic moment (1). The long-range antiferromagnetic order and μ_{Cu} -- as well as any tensile stress on the Cu-O bonds -- disappears with an increasing electron concentration in the σ^* bands. Therefore these materials can be doped n-type. Moreover, square-coplanar coordination is not optimal for Cu^{2+} ions; it would appear that the electrons may become trapped as large polarons by a dynamic bending of the Cu-O-Cu bond angles from 180°. Thus n-type superconductivity can be stabilized and have a high T_c due to enhanced electron-lattice coupling where the Cu-O-Cu bond angle is 180°. Why there should be an abrupt transition from an antiferromagnetic semiconductor to an n-type superconductor in a narrow compositional interval is not clear. It would appear that the retention of a correlation splitting is playing a fundamental role.

In summary, a survey of electronic-conduction processes in solid oxides has been outlined and applied to the problem of high-T_c superconductivity in ceramic materials. The peculiar structural features of the perovskites have been highlighted in an attempt to identify the origin of the enhanced pairing potential of the superconductive pairs in perovskite-related structures. The competitive nature vis a vis superconductivity of CDWs or a correlation splitting associated with spontaneous atomic moments has also been stressed.

REFERENCES

1. J. B. Goodenough, Am. Chim. Fr. 7, 459 (1962).
2. C. Chaillout, A. Santoro, J.P. Remeika, A.S. Cooper, G.P. Espinosa, and M. Marezio, Solid State Comm. *65*, 1363 (1988).
3. J. B. Goodenough, Progress Solid-State Chemistry *5*, 145 (1972).
4. R.J. Cava, B. Batlogg, J. Krajewski, R C. Ferrel, L.W. Rupp, A.E. White, W.F. Peck, and T.W. Kometani, Nature (London) *332*, 814 (1988).
5. L.F. Mattheiss, E.M. Gyorgy, and D.W. Johnson, Phys. Rev. B *37*, 3745 (1988).
6. D.G. Hinks, B. Dabrowski, J.D. Jorgensen, A.W. Mitchell, D.R. Richards, S. Pei, and D. Shi, Nature (London) *333*, 836 (1988).
7. J.P. Wignacourt, J.S. Swinnea, H. Steinfink, and J. B. Goodenough, Appl. Phys. Lett. *53*, 1753 (1988).
8. M.S. Hegde, P. Barboux, C.C. Chang, J.M. Tarascon, T. Venkatesan, X.D. Wu, and A. Inman, Phys. Rev. B*39*, 4752 (1989).
9. M.R. Oliver, J.O. Dimmock, A.L. McWhorter, and T.B. Reed, Phys. Rev. B*5*, 1078 (1972).
10. J. B. Goodenough in "Defects and Transport in Oxides," M.S. Seltzer and R.J. Jaffee, eds (Plenum Publ. Co., New York, 1974) p. 55.
11. J. B. Goodenough in "Physics and Chemistry of Electrons and Ions in Condensed Matter," J.V. Acrivos et al eds (D. Reidel Publ. Co., Amsterdam, 1984) p. 1.
12. J. B. Goodenough, M. M. Thackeray, W.I.F. David, and P.G. Bruce, Rev. Chim. minerale *21*, 435 (1984).
13. J. B. Goodenough in "Proceedings of Climax Fourth International Conference on the Chemistry and Uses of Molybdenum," H.F. Barry and P.C.H. Mitchell, eds (Climax Molybdenum Co., Ann Arbor, 1982) p. 1.
14. H. Takagi, S. Uchida, K. Kitazawa, and S. Tanaka, Jpn. J. Appl. Phys. *26*, L123 (1987).
15. J.D. Jorgensen, H-B Schuttler, D.G. Hinks, D.W. Capone II, K. Zhang, M.B. Brodsky, and D.J. Scalapino, Phys. Rev. Lett. *58*, 1024 (1987).
16. J.B. Torrance, Y. Tokura, A.J. Nazzal, A. Bezinge, T.C. Huang, and S.S.P. Parkin, Phys. Rev. Lett. *61*, 1127 (1988).
17. R. Yoshizaki, N. Ishikawa, M. Akamatsu, J. Fujikami, H. Kurahashi, Y. Saito, Y. Abe, and H. Ikeda, Physica C *156*, 297 (1988).
18. Y. Kitaoka, K. Ishida, S. Hiramatsu, and K. Asayama, J. Phys. Soc. Japan 57, 734 (1988).
19. R.J. Birgeneau, D.R. Gabbe, H.P. Jenssen, M.A. Kastner, P. J. Picone, T.R. Thurston, G. Shirane, Y. Endoh, M. Sato, K. Yamada, Y. Hidaka, M. Oda, Y. Enomoto, M. Suzuki, and T. Murakami, Phys. Rev. B*38*, 6614 (1988).
20. L.F. Mattheiss, Phys. Rev. Lett. *58*, 1028 (1987).
21. J. Yu, A.J. Freeman, and J-H Xu, Phys. Rev. Lett. *58*, 1035 (1987).
22. Y. Guo, J-M. Langlois and W.A. Goddard, Science *239*, 896 (1988).
23. D. Vaknin, S.K. Sinha, D.E. Moncton, D.C. Johnston, J.M. Newsam, C.R. Safinya, and M.E. King, Jr., Phys. Rev. Lett. 58, 2802 (1987).
24. T. Freltoft, J.E. Fischer, G. Shirane, D.E. Moncton, S.K. Sinha, D. Vaknin, J.P. Remeika, A.S. Cooper, and D. Harshman, Phys. Rev. B*36*, 826 (1987).
25. N. Nucker, J. Fink, J.C. Fuggle, P.J. Durham, and W.M. Temmerman, Phys. Rev. B*37*, 5158 (1988).
26. F.J. Himpsel, G.V. Chandrashekar, A.B. McLean, and M.W. Shaefer, Phys. Rev. B*38*, 11946 (1988).
27. Y. Dai, A. Manthiram, A. Campion and J.B. Goodenough, Phys. Rev. B*38*, 5091 (1988).
28. J. Zhou, S. Sinha, and J.B. Goodenough, Phys. Rev. B (in press).
29. J.B. Goodenough and A. Manthiram, Physica C *157*, 439 (1989).

30. J.D. Jorgensen, B. Dabrowski, S. Pei, D.R. Richards, and D.G. Hinks, Phys. Rev. B (submitted).

31. C. Chaillout, S.W. Cheng, Z. Fisk, M.S. Lehmann, M. Marezio, B. Morosin, and S.E. Schirber, Physica C (submitted).

32. M.W. Shaefer, T. Penney, B.L. Olson, R.L. Greene, and R.H. Koch, Phys. Rev. B39, 2914 (1989) and references therein; Y.T. Jeanne et al, Phys. Rev Lett. 63, 2318 (1989)

33. J.B. Goodenough, Mater. Res. Bull 23, 401 (1988).

34. J.B. Goodenough and J.M. Longo, Landolt-Börnstein Tabellen *III/4a*, 126 (1970).

35. J. Gopalkrishnan, M.A. Subramanion, C.C. Torardi, J.P. Attfield, and A.W. Sleight, Mater. Res. Bull. (~~in press~~). 24, 33 (1989)

36. T. Tokura, H. Takagi, and S. Uchida, Nature *337*, 345 (1989).

37. H. Takagi, S. Uchida, and Y. Tokura, Phys. Rev. Lett. *62*, 1197 (1989).

38. A.C.W.P. James, S.M. Zahurak, and D.W. Murphy, Nature (~~in press~~) 338, 240 (1989)

39. J.T. Markert and M.B. Maple, Solid State Comm. (~~in press~~) 70, 145 (1989)

FIGURE CAPTIONS

Fig. 1 Construction of electron energies for MgO: (a) free ions, (b) point-charge solid, (c) crystal, (d) energy density of one-electron states.

Fig. 2 Schematic energy-densities of one-electron states N(E) vs energy E for three cubic perovskites (a) $BaSnO_3$, (b)$BaPbO_3$, and (c) hypothetical $BaBiO_3$.

Fig. 3 Oxygen-atom displacements from ideal-perovskite positions in monoclinic $BaBiO_3$.

Fig. 4 (a) Fermion energies and (b) transition temperatures vs like-atom interatomic resonance integral b for half-filled band with relatively small free-atom U.

Fig. 5 Tentative phase diagram for the system $Ba_{1-x}K_xBiO_3$.

Fig. 6 Schematic of $4f^n$-manifold energies relative to the energies of the conduction and valence bands of (a) GdO, (b) EuO, (c) $Eu_{1.8}O$, and (d) $EuO_{1.6}$.

Fig. 7 Construction of electron energies for MnO.

Fig. 8 Comparison of 3d-electron energies for (a) metallic TiO, (b) semimetallic VO, and (c) antiferromagnetic MnO.

Fig. 9 (a) Fermion energies and (b) transition temperatures vs like-atom interatomic resonance intergral b for half-filled band with a relatively large free-atom U.

Fig. 10 Comparison of 3d-electron energies for three mixed-valent systems: (a) $Li[Ti_2]O_4$, (b) Na_xWO_3, and (c) $Li[Mn_2]O_4$.

Fig. 11 (a) Tetragonal T structure of $La_{1.85}Sr_{0.15}CuO_4$ and (b) oxygen displacements below the orthorhombic-tetragonal transition-temperature T_t.

Fig. 12 Tentative phase diagram for the system $La_{2-x}Sr_xCuO_4$.

Fig. 13 Schematic density of one-electron states vs energy for stoichiometric La_2CuO_4: (a) uncorrelated band calculations, (b) with correlation splitting of the Cu(II/I) and Cu(III/II) couples, and (c) origin of formal-valence ambiguity associated with "Cu(III)" states.

Fig. 14 Room-temperature lattice parameters vs quench temperatures for $La_2CuO_{4.05}$ heated successively to higher temperatures before quenching.

Fig. 15 Tetragonal T' structure of Nd_2CuO_4.

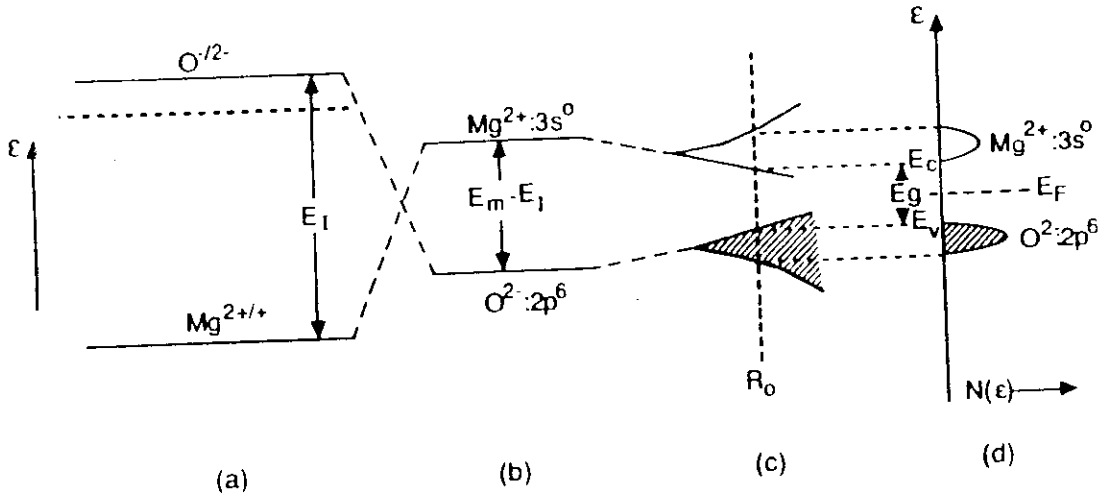
ε
$O^{-/2-}$
$Mg^{2+:}3s^o$
E_m-E_I
E_I
$Mg^{2+/+}$
O^{2-}:$2p^6$
R_o
E_c
E_g
E_F
E_v
Mg^{2+}:$3s^o$
O^{2-}:$2p^6$
N(ε)
(a)
(b)
(c)
(d)

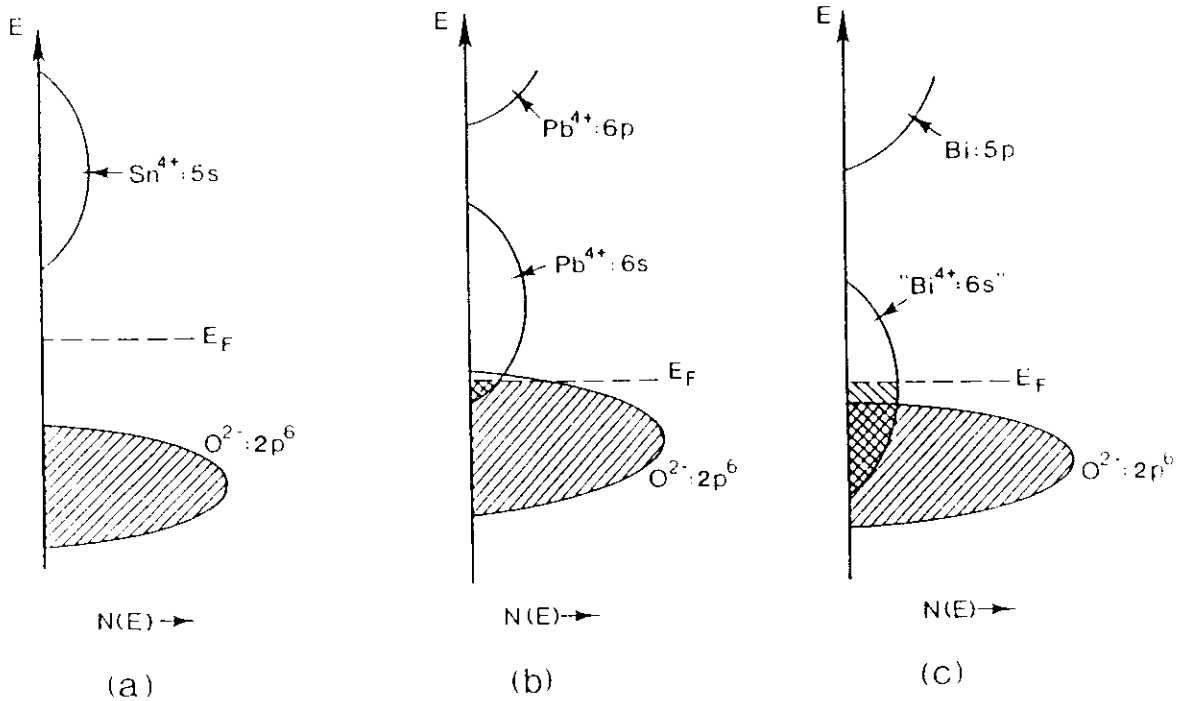
E
Sn^{4+}:5s
E_F
O^{2-}:$2p^6$
N(E)
(a)
E
Pb^{4+}:6p
Pb^{4+}:6s
E_F
O^{2-}:$2p^6$
N(E)
(b)
E
Bi:5p
"Bi^{4+}:6s"
E_F
O^{2-}:$2p^6$
N(E)
(c)

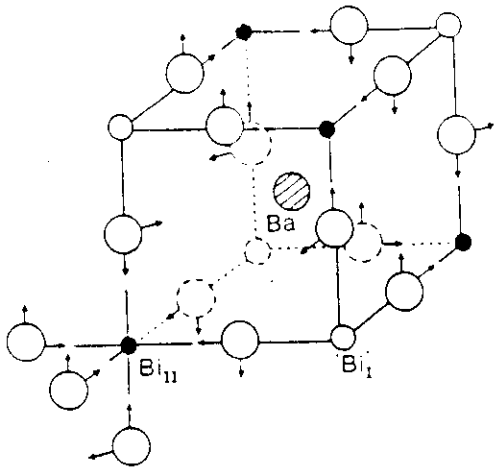
Ba
Bi_{II}
Bi_{I}

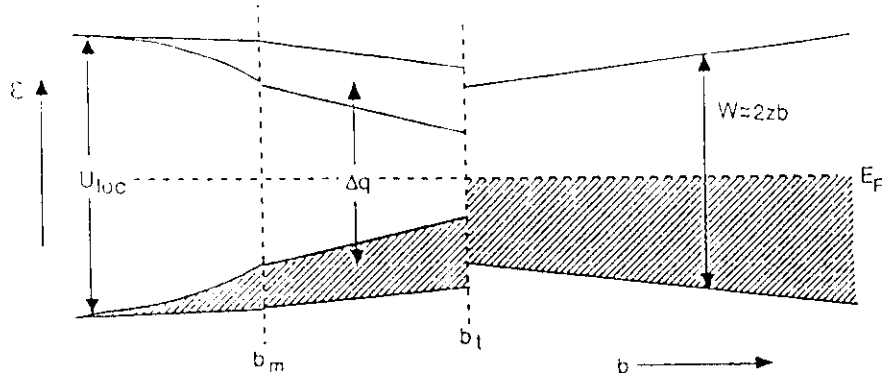
ε
U_{loc}
Δq
W≈2zb
E_F
b_m
b_t
b

(a)

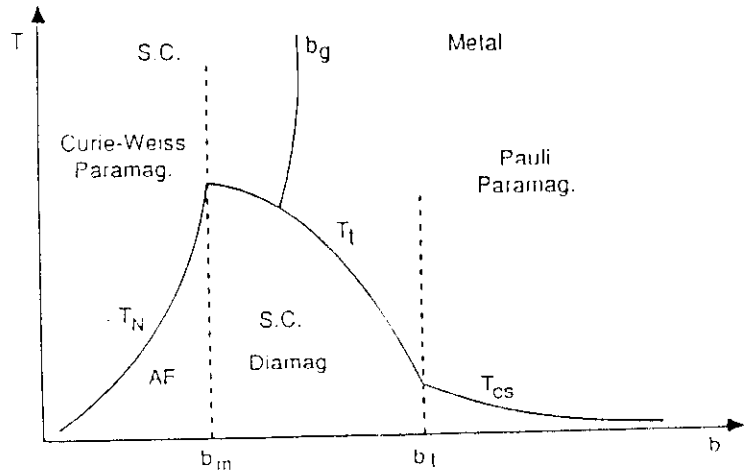
T
S.C.
b_g
Metal
Curie-Weiss
Paramag.
Pauli
Paramag.
T_t
T_N
S.C.
Diamag
AF
T_{cs}
b_m
b_t
b

(b)

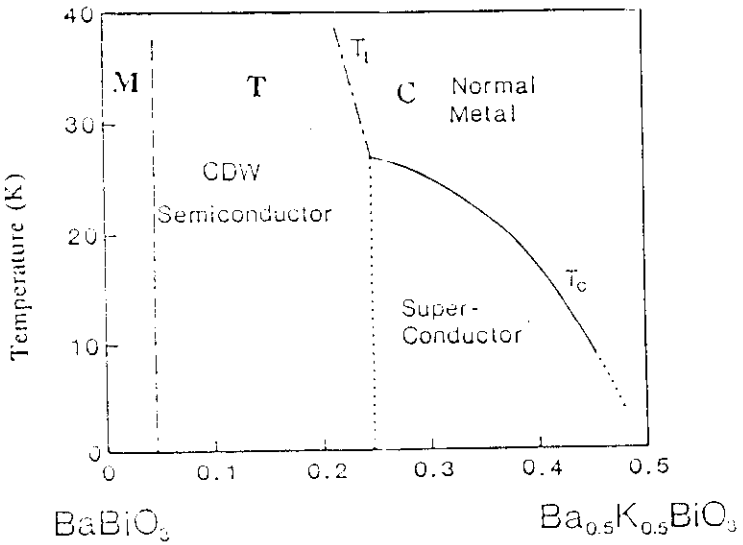
Temperature (K)
40
30
20
10
0
M
T
C
Normal Metal
T_t
CDW
Semiconductor
T_c
Super-Conductor
0
0.1
0.2
0.3
0.4
0.5
$BaBiO_3$
$Ba_{0.5}K_{0.5}BiO_3$

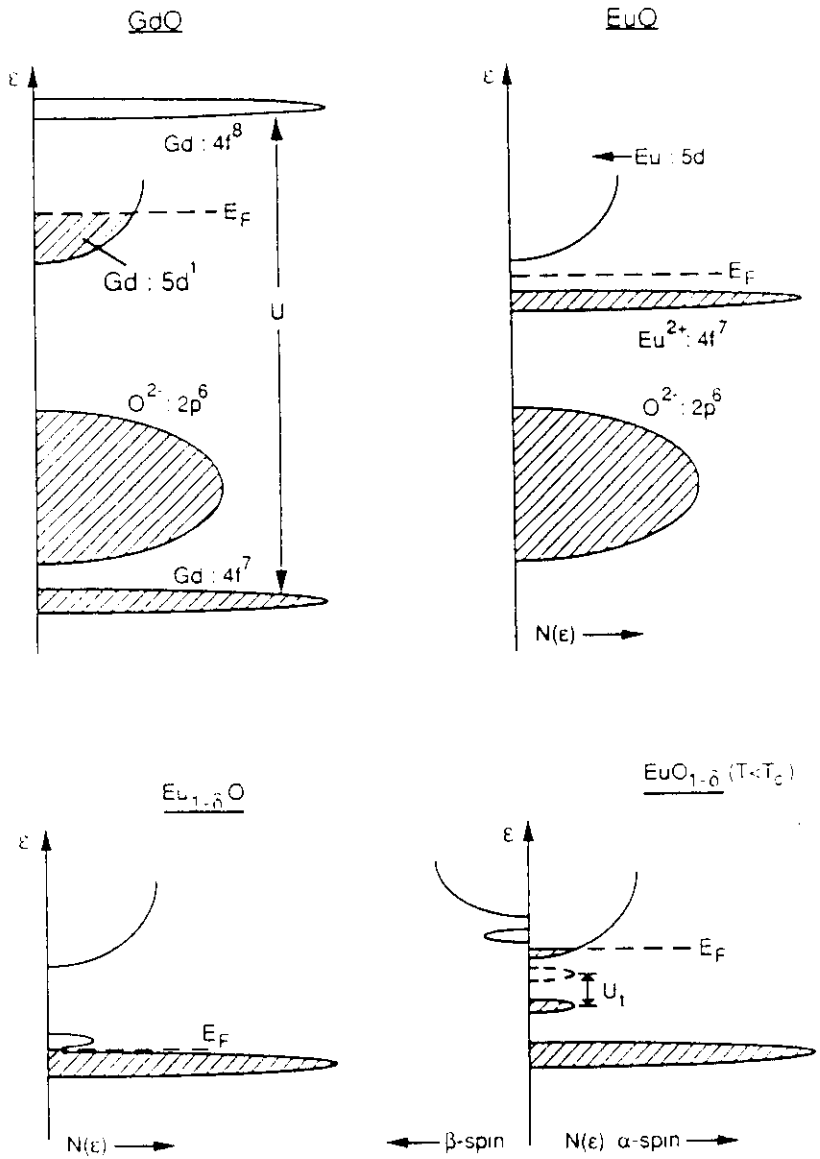
GdO
ε
Gd : $4f^8$
E_F
Gd : $5d^1$
U
O^{2-} : $2p^6$
Gd : $4f^7$
EuO
ε
Eu : 5d
E_F
Eu^{2+} : $4f^7$
O^{2-} : $2p^6$
N(ε)
$Eu_{1-\delta}O$
ε
E_F
N(ε)
$EuO_{1-\delta}$ ($T<T_c$)
ε
E_F
U_1
β-spin
N(ε) α-spin

MnO

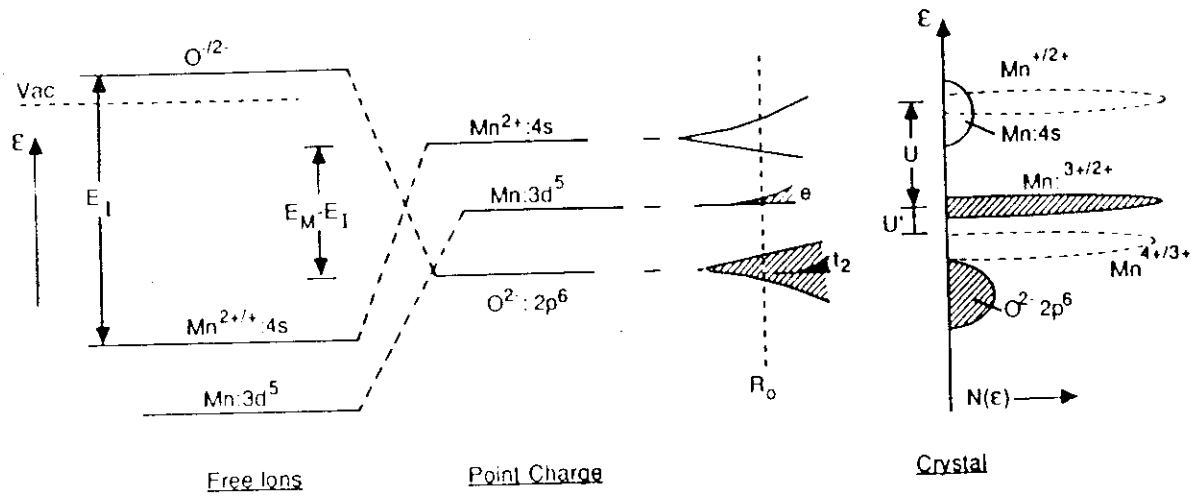
Vac
ε
$O^{-/2-}$
E_I
E_M-E_I
$Mn^{2+/+}$:4s
Mn:$3d^5$
Mn^{2+}:4s
Mn:$3d^5$
O^{2-}:$2p^6$
e
t_2
R_o
ε
$Mn^{+/2+}$
Mn:4s
U
U'
Mn:$^{3+/2+}$
$Mn^{4+/3+}$
O^{2-} $2p^6$
N(ε)
Free Ions
Point Charge
Crystal

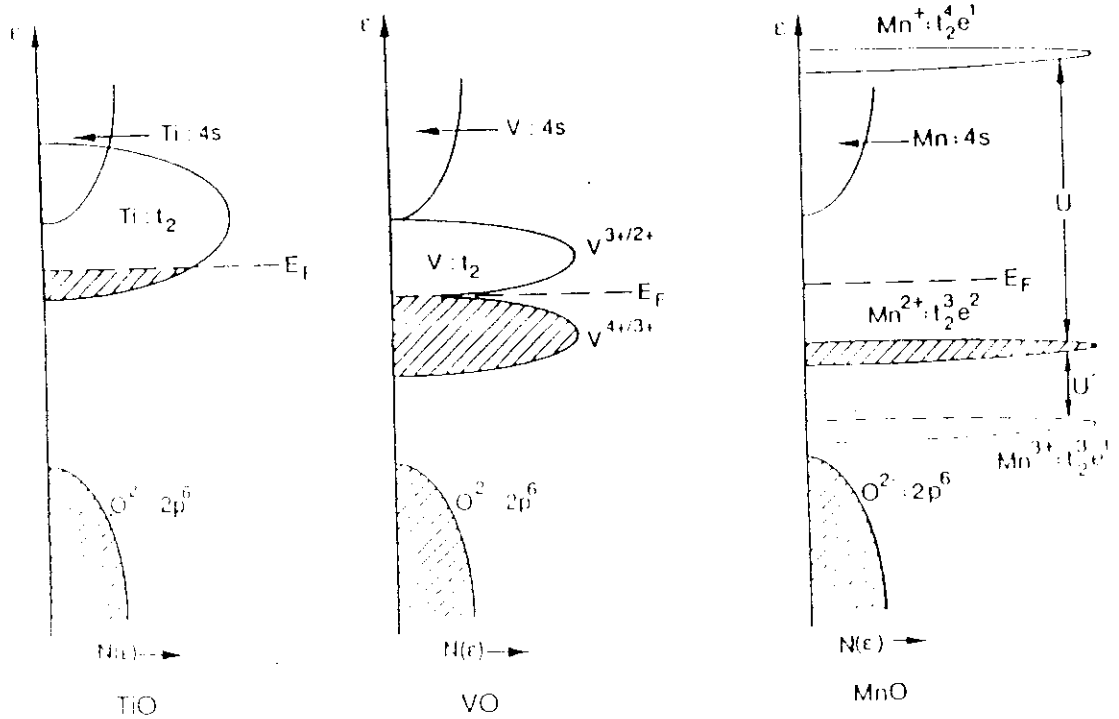
Ti : 4s
Ti : t_2
E_F
O^{2-} $2p^6$
N(ε)
TiO
V : 4s
V : t_2
$V^{3+/2+}$
E_F
$V^{4+/3+}$
O^{2-} $2p^6$
N(ε)
VO
Mn^{+}:$t_2^4e^1$
Mn : 4s
U
E_F
Mn^{2+}:$t_2^3e^2$
U'
Mn^{3+}:t_2^3
O^{2-} : $2p^6$
N(ε)
MnO

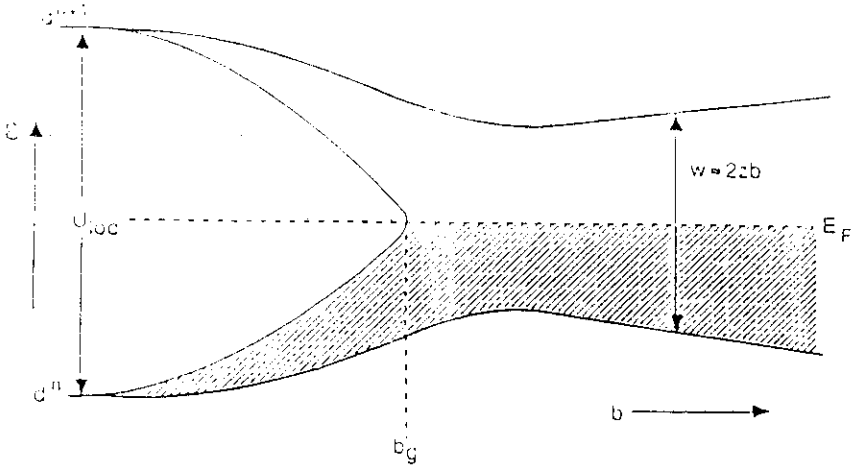
ε
U_{loc}
E_F
w = 2zb
b
b_g

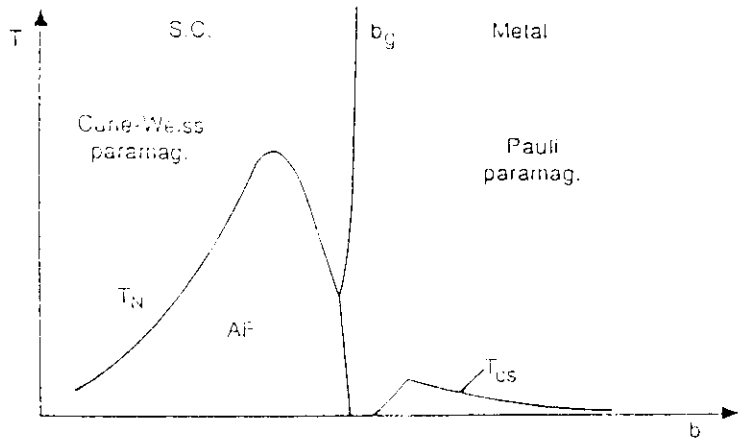
T
S.C.
b_g
Metal
Curie-Weiss
paramag.
Pauli
paramag.
T_N
AF
T_{cs}
b

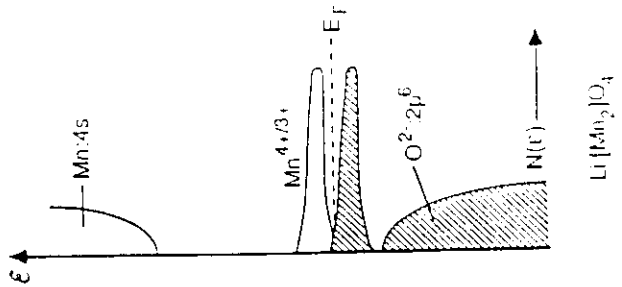
Mn:4s
$Mn^{4+/3+}$
E_F
$O^{2-}:2p^6$
N(ε)
ε
$Li[Mn_2]O_4$

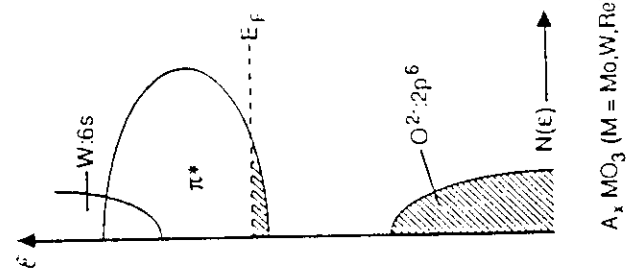
W:6s
π*
E_F
$O^{2-}:2p^6$
N(ε)
ε
$A_x MO_3$ (M = Mo,W,Re)

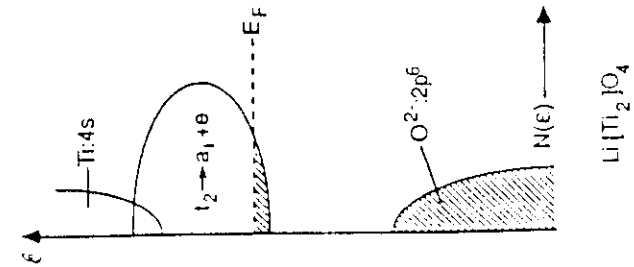
Ti:4s
$t_2 \rightarrow a_1 + e$
E_F
$O^{2-}:2p^6$
N(ε)
ε
$Li[Ti_2]O_4$

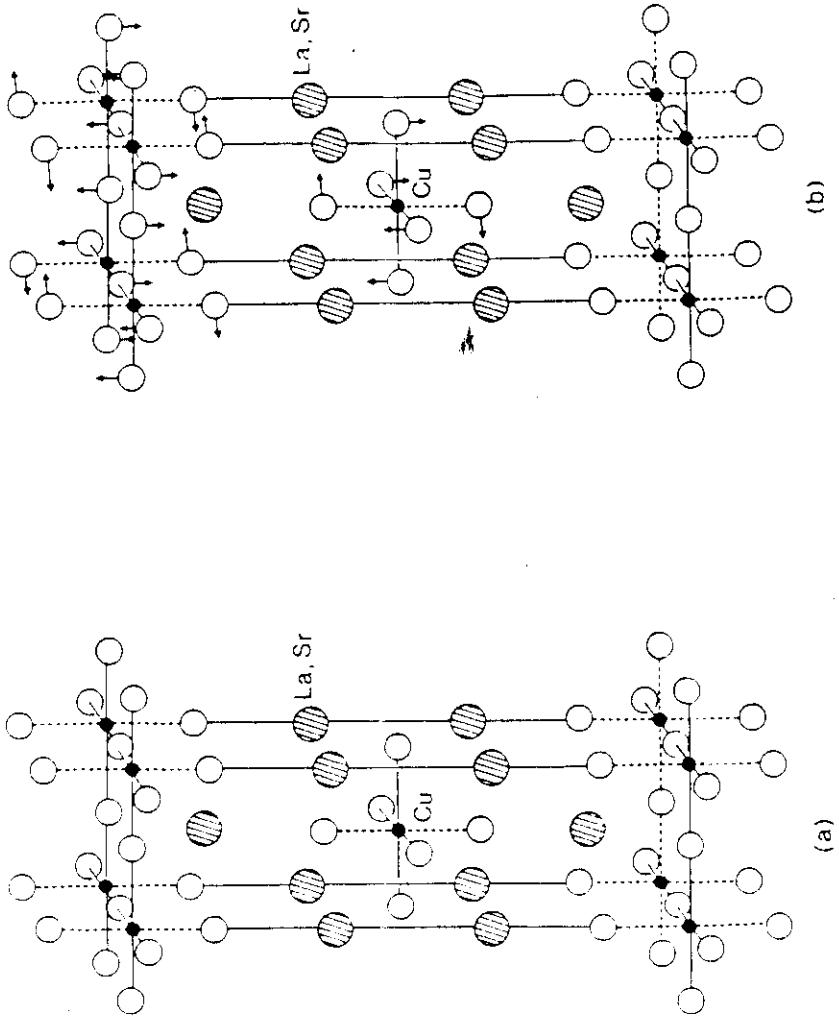
La, Sr
Cu
(b)
La, Sr
Cu
(a)

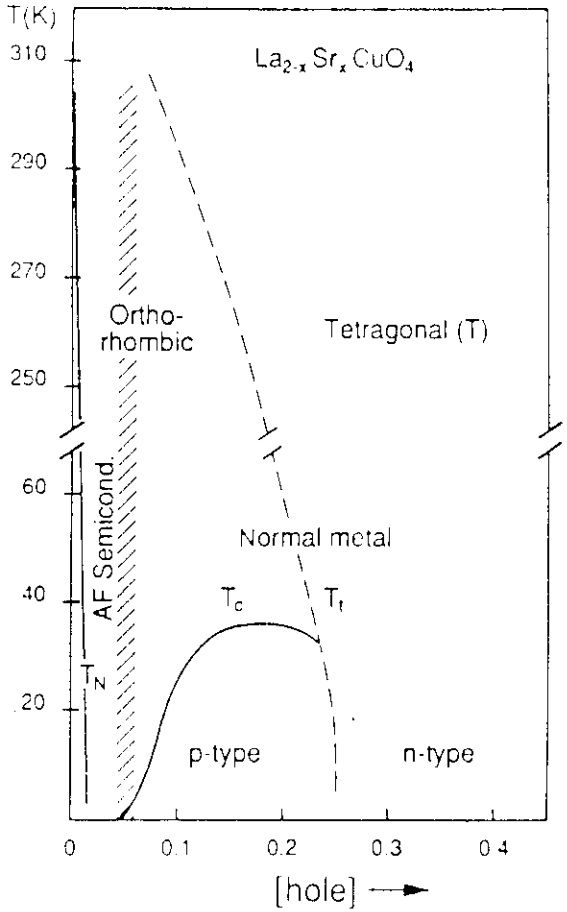
T(K)
310
290
270
250
60
40
20
$La_{2-x}Sr_xCuO_4$
Ortho-
rhombic
Tetragonal (T)
AF Semicond.
Normal metal
T_c
T_f
T_N
p-type
n-type
0
0.1
0.2
0.3
0.4
[hole] ⟶

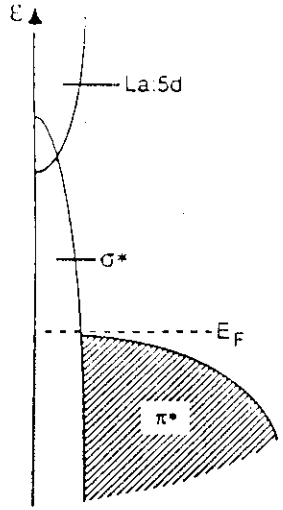

Uncorrelated
(a)

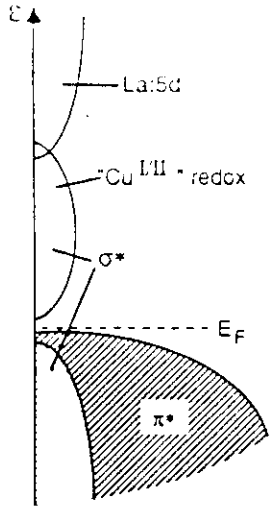

Correlated (AF)
(b)

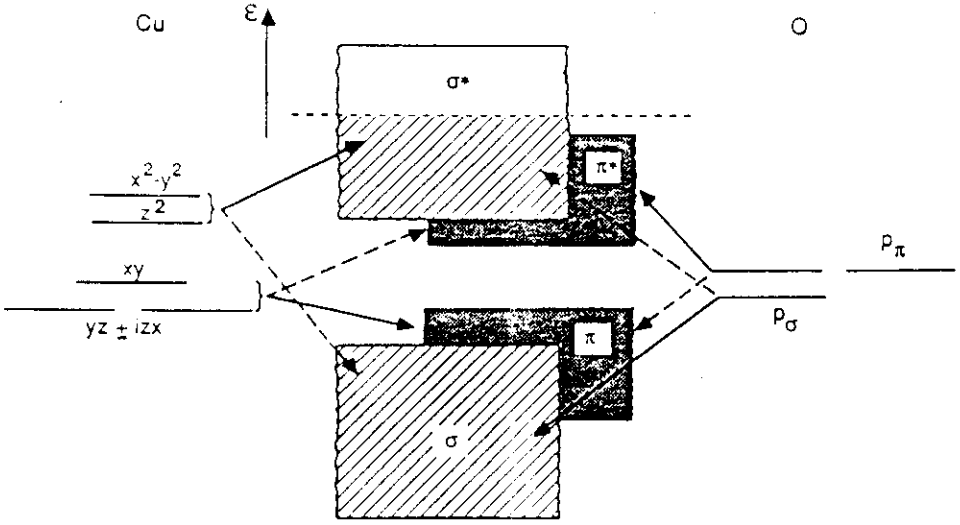

(c)